High-fidelity simulations of the mixing and combustion of a technically premixed hydrogen flame

D.Mira[a,*], A. Both[a], O. Lehmkuhl[a], S. Gomez[a], J. Forck[b], T. Tanneberger[b], P. Stathopoulos[b,c], C.O. Paschereit[b]

[a] *Barcelona Supercomputing Center (BSC), Barcelona, Spain.*
[b] *Technische Universität Berlin (TUB), Berlin, Germany.*
[c] *Deutsches Zentrum für Luft- und Raumfahrt e.V. (DLR), Berlin, Germany.*

Abstract

Numerical simulations are used here to obtain further understanding on the flashback mechanism of a technically premixed hydrogen flame operated in lean conditions. Recent work from the authors (Mira et al., 2020) showed that the hydrogen momentum strongly influences the flame dynamics and plays a fundamental role on the stability limits of the combustor. The axial injection influences the vortex breakdown position and therefore, the propensity of the burner to produce flashback. This work is an extension of our previous work where we include a detailed description of the mixing process and the influence of equivalence ratio fluctuations and heat loss on the flame dynamics.

Keywords:
hydrogen, turbulent flame, large-eddy simulations, flamelets

1. Introduction

The combustion of hydrogen-enrich fuels in gas turbines is a highly investigated topic [1], with the potential to contribute significantly to the decarbonization of a variety of energy applications [2–4]. This potential comes with the demand on future burner designs to accommodate a multitude of fuels with varying, but high, amounts of hydrogen [5], while allowing for a wide stability range, high efficiency and low NO_x emissions. From these requirements, the investigation of burner designs to operate on pure hydrogen can establish a benchmark for many upcoming high-reactivity fuel combustors, leading to insights that can have a significant effect on a wide variety of future energy applications.

Flame stabilization is one of the major factors to be considered for the safe operation of hydrogen gas turbine burners. A burner design to operate with hydrogen-air mixtures building upon the concept of central non-swirling axial air injection (AI) for Flashback (FB) prevention was developed by Reichel et al. [6–9]. This burner concept was introduced by Burmberger and Sattelmayer [10] and it is used in this burner to increase the operational range when operated with hydrogen. This burner design is particularly interesting for high reactivity fuels like hydrogen or syngas, which are prone to FB in conventional swirl stabilized burners as reported by Mayer et al. [5].

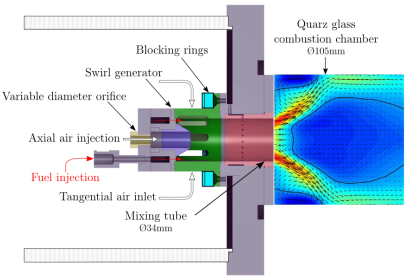

Figure 1: Schematic of burner model, indicating different volume flow pathways through swirl generator or axial injection.

The burner geometry, see Fig. 1, was studied experimentally by Reichel et al. [6–9] with the goal of finding a configuration for extending stability limits set by FB. The investigation was primary focused on driving mechanisms influencing FB as well as their inter-dependencies. In particular, the influence of fuel momentum and AI on FB resistance were assessed. It was shown that without AI, the central recirculation zone (CRZ) caused by the vortex break down (VB), which is necessary for flame

*Corresponding author: Daniel Mira, BSC.
Email address: daniel.mira@bsc.es (D.Mira)

anchoring, extends close or even into mixing tube for some operating conditions, showcasing a deficit in axial velocity on the central axis of the mixing tube. This is typical for high swirl, low-reacting fuel combustors [11, 12], but can lead to FB if high reacting fuels are used [5]. Using different rates of AI, which can be quantified by the ratio of axially injected, non-swirling air flow to total air flow $\chi = \dot{V}_{\mathrm{ax}}/(\dot{V}_{\mathrm{ax}} + \dot{V}_{\mathrm{swirl}})$, it could be shown for a medium AI rate ($\chi = 7.5\%$) that it overcomes the axial velocity deficit partially over the length of the mixing tube, while not pushing the VB further downstream. In contrast, a high rate of AI ($\chi = 12.5\%$) could overcome the axial velocity deficit over the whole mixing tube pushing the VB downstream into the combustion chamber. This strategy allows an increase in FB resistance, as the flow profile at the mixing tube outlet approaches the ideal plug-like flow shape [7], which was also demonstrated by numerical simulations in the work by Mira et al. [13]. Reichel et al. [7] have shown that the AI reduces the initial swirl number. Note that high swirl ensures a compact flame attached to the burner exit, but lower swirl is favourable for FB resistance due to simpler axial velocity deficit compensation.

Another dominant parameter influencing the flame stabilization in this burner is the fuel momentum that is introduced by the high-speed injection of hydrogen. Since hydrogen has a very low amount of energy density, volume flow rates are very high compared to conventional fuels like natural gas, to account for a similar thermal power output. The momentum ratio J, as described in Reichel et al. [9] can be used to quantify the amount of axial injection featured in the burner. Note the momentum ratio increases with increase in equivalence ratio ϕ for a constant air mass flow rate. If compared to natural gas, hydrogen yields a momentum ratio that is 37% higher assuming the same combustor power and taking differences in volumetric heating value and molecular mass into account [9]. The hydrogen injection upstream of the mixing tube also contributes to lowering the resulting swirl number at the mixing tube outlet, though it is not able to overcome the axial velocity deficit at the center of the mixing tube without the AI ($\chi = 0$). Only when including AI, an increase in FB resistance is found. In fact, the experimental results showed that higher equivalence ratios cause a downstream shift of the stagnation point, therefore increasing FB resistance [9]. These observation were also confirmed by numerical simulations using a perfectly premixed assumption in a previous work from the same authors [13], where the flow field and flame stabilization were well predicted imposing the same axial momentum as in the technically premixed case. In this case, the additional fuel momentum gained by higher equivalence ratios has a more significant impact on the flow field then the increased reactivity. It can be summarized that AI and fuel momentum can promote the favourable plug-like flow shape at the outlet of the mixing tube, while featuring a CRZ and pushing the stagnation point into the combustion chamber contributing to additional FB resistance.

This work is an extension of our previous work [13] where the hydrogen-air mixing is accounted for and the impact of fluctuations in equivalence ratio and fuel heterogeneity are analysed. The paper is structured as follows. A description of the modelling approach is presented in the next section and the computational cases considered for the inert and reacting flow problems are then described. The results section is followed by a detailed description of the mixing process and preliminary results of the reacting flow field for a stable operating point is presented and discussed. Finally, some conclusions and directions of future work are given.

2. Modelling approach

2.1. Governing equations

The equations describing the flow field correspond to the low-Mach number approximation of the Navier-Stokes equations with the energy equation represented by the total enthalpy. The Favre-filtered governing equations for LES correspond to the continuity, momentum and enthalpy and read as:

$$\frac{\partial \bar{\rho}}{\partial t} + \boldsymbol{\nabla} \cdot (\bar{\rho}\tilde{\boldsymbol{u}}) = 0, \tag{1}$$

$$\frac{\partial \bar{\rho}\tilde{\boldsymbol{u}}}{\partial t} + \boldsymbol{\nabla} \cdot (\bar{\rho}\tilde{\boldsymbol{u}}\tilde{\boldsymbol{u}}) = -\boldsymbol{\nabla} \cdot \overline{\tau}_M - \boldsymbol{\nabla}\bar{p} + \boldsymbol{\nabla} \cdot (\bar{\mu}\boldsymbol{\nabla}\tilde{\boldsymbol{u}}), \tag{2}$$

$$\frac{\partial \overline{\rho}\tilde{h}}{\partial t} + \boldsymbol{\nabla} \cdot \left(\overline{\rho}\tilde{\boldsymbol{u}}\tilde{h}\right) = -\boldsymbol{\nabla} \cdot \overline{\tau}_h + \boldsymbol{\nabla} \cdot \left(\bar{\rho}\bar{D}\boldsymbol{\nabla}\tilde{h}\right), \tag{3}$$

where standard notation is used for all the quantities with $\bar{\rho}$, $\tilde{\boldsymbol{u}}$, $\tilde{h}$, $\bar{D}$, $\bar{p}$ and $\bar{\mu}$ represent the density, velocity vector, total enthalpy (sensible and chemical), diffusivity, pressure and dynamic viscosity using filtered quantities. The τ term stands for the unresolved or subgrid terms related to the filtering operation and applies to the unresolved momentum flux $\overline{\tau}_M$ and the unresolved enthalpy flux $\overline{\tau}_h$. The subgrid viscous stress tensor is determined based on the Stoke's assumption and the turbulence contribution is obtained by the use of the Boussinesq approximation [14]. A unity Lewis number assumption has been made to simplify the scalar transport in the governing equations. Heating due to viscous forces is neglected in the enthalpy equation and the unresolved heat flux is modelled using a gradient diffusion approach [15]. The

modelling framework is closed by an appropriate expression for the subgrid-scale viscosity. The eddy-viscosity is obtained from the Vreman [16] model using a constant $c_k = 0.1$. The same single-value constant has been used in previous studies and it is also retained here [13, 17]. The flame structure of this non-premixed flame is determined by the flamelet method [13]. Based on the characteristics of the mixing field, a comparison of the tabulation of premixed laminar flames and counterflow diffusion flames for the construction of the thermochemical database is undertaken, though the results presented here will only include those based on diffusion flamelets. An unsteady extinguishing flamelet is used as a natural continuation of this two-dimensional manifold [18]. The flamelet database uses the chemistry from the full San Diego mechanism (Chemical-Kinetic Mechanisms for Combustion Applications [19]), which demonstrated excellent performance for predicting hydrogen flames in a variety of flow conditions [13, 15, 20] and is also retained here. The effects of heat loss on the flamelet database are considered by the tabulation of strained diffusion flames at different enthalpy levels. Three controlling variables are used to characterize the thermochemical state of the flamelets composing the manifold: mixture fraction Z, progress variable Y_c, and normalized enthalpy i. In order to account for turbulent/chemistry interactions at the subgrid scale, the tabulated properties from the manifold are integrated with a presumed-shape probability density function (PDF) that describes the statistical effect of turbulence on the flame structure [21]. The systems of equations read:

$$\frac{\partial \overline{\rho}\tilde{Z}}{\partial t} + \boldsymbol{\nabla}\cdot\left(\overline{\rho}\tilde{\boldsymbol{u}}\tilde{Z}\right) = -\boldsymbol{\nabla}\cdot\overline{\tau}_Z + \boldsymbol{\nabla}\cdot\left(\bar{\rho}\bar{D}\boldsymbol{\nabla}\tilde{Z}\right), \quad (4)$$

$$\frac{\partial \overline{\rho}\tilde{Y_c}}{\partial t} + \boldsymbol{\nabla}\cdot\left(\overline{\rho}\tilde{\boldsymbol{u}}\tilde{Y_c}\right) = -\boldsymbol{\nabla}\cdot\overline{\tau}_{Y_c} + \boldsymbol{\nabla}\cdot\left(\bar{\rho}\bar{D}\boldsymbol{\nabla}\tilde{Y_c}\right) + \overline{\dot{\omega}}_{Y_c}, \quad (5)$$

$$\frac{\partial \overline{\rho}Z_v}{\partial t} + \boldsymbol{\nabla}\cdot\left(\overline{\rho}\tilde{\boldsymbol{u}}Z_v\right) = -\boldsymbol{\nabla}\cdot\overline{\tau}_{Z_v} + \boldsymbol{\nabla}\cdot\left(\bar{\rho}\bar{D}\boldsymbol{\nabla}Z_v\right) - 2\overline{\tau}_Z\cdot\boldsymbol{\nabla}\tilde{Z} - 2\overline{s}_{\chi Z}. \quad (6)$$

The unresolved terms $\overline{\tau}_Z$ and $\overline{\tau}_{Y_c}$ are closed using a gradient diffusion approach [21]. The term $\overline{\dot{\omega}}_{Y_c}$ is the filtered progress variable source term and $\overline{s}_{\chi Z}$ is the unresolved part of the scalar dissipation rate, which is modeled assuming a linear relaxation of the variance within the subgrid [21].

3. Computational cases

The operating conditions considered in this study correspond to a lean point at equivalence ratio $\phi = 0.6$ during stable operation. The burner operates with a Reynolds number Re = 75000 based on the mixing tube diameter with pre-heated air at T_{air} = 453K and hydrogen coming at T_{H2} = 320K. Geometrical details of the burner and additional parameters describing the operating point can be found in the experimental papers [6–9] and our previous numerical work [11–13].

For the mixing analysis, an evaluation of different aspects going from the resolution of the mesh, a simplification of the fuel injection and including Lewis number effects using constant Lewis number (Le) in the mixture fraction and subgrid variance transport equation are considered. The baseline case (BL) corresponds to the case with unity Lewis number, the fuel injection directly on the boundary patch with 16 holes, and the reference mesh with resolution of 0.4 mm in the mixing tube, see[13] for further information about this mesh. The rest of cases includes variation in these parameters and the fine mesh includes a resolution in the upstream part of the mixing tube of 0.1 mm to better resolve the mixing process. A summary of the test cases is given in Table 1. The reacting cases include two cases considering the full domain, the reference mesh and unity Lewis number including an adiabatic and non-adiabatic case respectively.

Table 1: Computational cases for the mixing analysis

Case	Le	Domain	Mesh
BL	1.0	Simple	Regular
C1D	1.0	Full	Regular
C1M	1.0	Simple	Fine
C1L	0.5	Simple	Regular

4. Results

In this section, results of the mixing analysis and the reacting flow field are presented. The study of mixing aims to evaluate the impact of modelling and numerical parameters on the development of the axial velocity profiles and mixture fraction distribution across the mixing tube. The reacting case describes the preliminary results of the flame comparing adiabatic and non-adiabatic calculations.

4.1. Mixing

As the fuel-air mixing plays an important role in flame dynamics and flashback resistance, a dedicated analysis of the mixing process is presented. Firstly, an study of the interaction between the fuel jets and the swirling

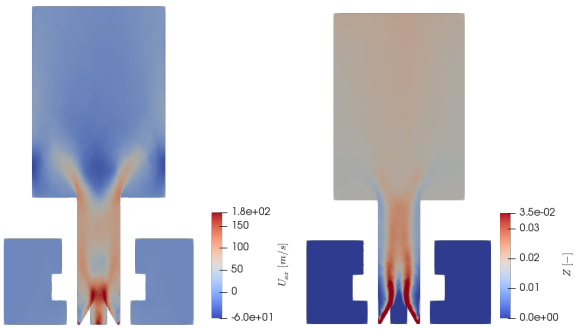

Figure 2: Time-averaged axial velocity (left) and mixture fraction (right) of BL-case in central plane.

air is conducted to evaluate the impact of the fuel momentum and fuel-air mixing on the velocity profiles and mixture fraction field across the mixing tube. The complete domain (Case C1D) is compared to a simplified configuration in which the fuel is directly injected into the boundary patches at constant flow rate. The fuel is injected in the upstream part of the mixing tube through 16 injection holes and the hydrogen is mixed with the swirling air. This partially premixed mixture forms a rich ring surrounding the AI. This interaction results in a region with high axial velocity that is attenuated as the flow develops downstream. The hydrogen concentration is shifted to the centerline of the mixing tube developing a partially premixed mixture that is richer on the central part, which is consistent with the experimental and numerical findings [8, 12]. The mixing field suggests the flame can exhibit equivalence ratio fluctuations, which do not introduce instabilities as found in the experiments [9] and numerical simulations[13]), but can influence the flame stabilization mechanisms. Looking at the axial velocity distribution at the mixing tube outlet it can be seen that the flow does not overcome the central axial velocity deficit over the whole length of the mixing tube. Therefore, the VB stabilizes just at the outlet of the mixing tube. Further analysis is devoted in the next subsection to this effect.

Considering the differences in magnitude of the transport properties for hydrogen and air, an assessment of the influence of diffusivity and viscosity on the mixing process was conducted. Preferential diffusion effects might influence the mixing and combustion process in turbulent flames [22], so this is examined here. The unity Lewis number approach is compared with a constant effective Lewis number $Le = 0.5$. As mentioned in Tab. 1), case C1L had the Lewis number set to $Le = 0.5$, while the species diffusion in case C1 was set to half the species diffusivity with $Le = 1$. Figure 3 shows the development of axial momentum in the mixing tube considering the 4 different cases.

Figure 3 exhibits few characteristics that illustrate the aforementioned descriptions. At the beginning of the mixing tube, the axial momentum of the case C1D is clearly higher than the rest of cases. This is due to the higher but unevenly distributed injection velocities, which differ from the BL-case in not being forced uniformly onto the boundary condition of the mixing tube. At approximately $z = 0.056\,[m]$ the axial momentum reaches its maximum, which can be attributed to the flow adapting to the end of the swirler veins. The spatial variations in axial momentum along the mixing tube correspond to variations in the velocity field across the mixing tube, see Fig. 2.

The swirl number is reduced as the flow approaches the combustion chamber. As discussed by Burmberger and Sattelmayer [10], a decline in swirl number is caused by a negative gradient of azimuthal velocity along the

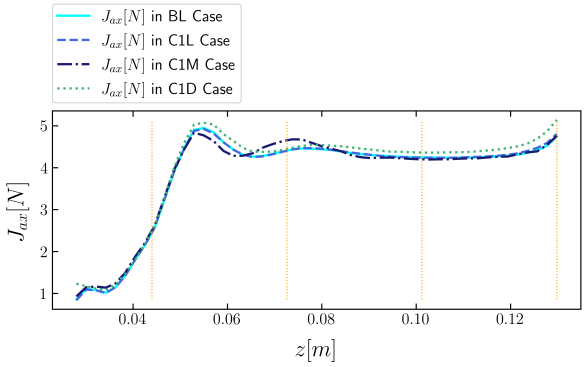

Figure 3: Comparison of axial momentum averaged over cross sections of the mixing tube (orange lines mark coordinates of specified cross section, see Fig. 5).

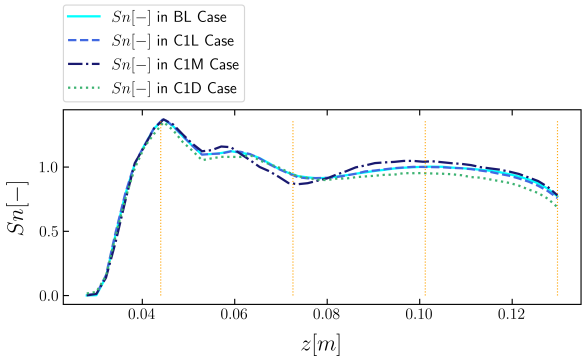

Figure 4: Comparison of swirl number averaged over cross sections of the mixing tube (orange lines mark coordinates of specified cross section, see Fig. 5).

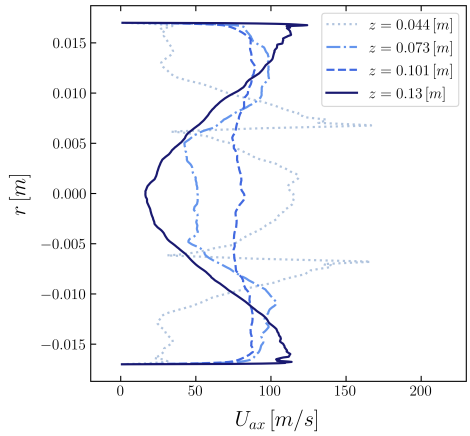

Figure 5: Velocity profiles along the mixing tube for BL-case.

mixing tube axis. The distribution of the swirl number for the different computational cases is shown in Fig. 4. To better understand this effect, the velocity profiles at different cross sections along the mixing tube are shown in Fig. 5. A velocity deficit along the center line is developed, which is partially influenced by the high hydrogen content in the central part that reduces the density. The description of the reacting flow fields for this flame is given in the next section.

4.2. *Reacting flow*

This section describes some preliminary results of the reacting flow field of the hydrogen flame. The flame can be distinguished in Fig. 6 by a contour plot of the velocity and progress variable fields at the middle plane of the burner during stable operation. A partially premixed mixture is exiting the mixing tube and a flame is stabilized by vortex breakdown in the combustion chamber. The flame is anchored by the central and corner recirculation zones and it is stabilized partially inside the mixing tube.

The proximity of the flame tip to the entrance of the combustion chamber develops an increase in axial velocity that provides resistance to flashback. The flame is burning around the global mixture fraction $Z_g = 0.017$, though it extends from $phi = 0.45$ to near stoichiometric conditions. The values of temperature conditioned to the mixture fraction can be used to identify the burning conditions, and this is shown in Fig. 7. The addition of heat loss has influenced the burning characteristics of the flame and more departure from equilibrium.

A comparison of the computed velocity field with the PIV data from Reichel et al., (2015) [8] along the centerline is shown in Fig. 8. It shows the simulations overpredict the maximum axial velocity at the mixing tube, which can be caused by a stabilization of the flame partially inside the mixing tube. After the flow expansion, the LES can capture the position of the VB and the size of the recirculation for the non-adiabatic case. The results show an improvement on the prediction of the flow field by adding heat loss to the combustion model. The maximum axial velocity after the expansion is reduced due to heat loss and the size of the central recirculation is also improved. The heat loss simulation is still unfinished and it is expected to further influence the velocity field. The mean velocity fields for the two cases at the middle plane is shown in Fig. 9. Further analysis and validation are currently performed.

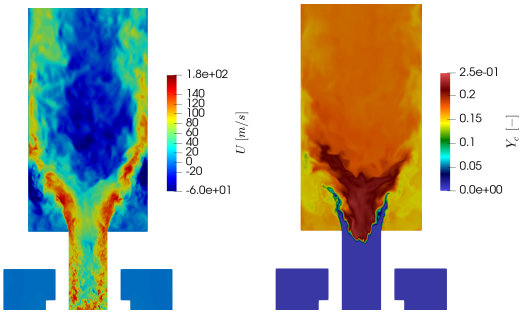

Figure 6: Axial velocity (left) and progress variable (right) fields of the flame including heat loss during stable burning.

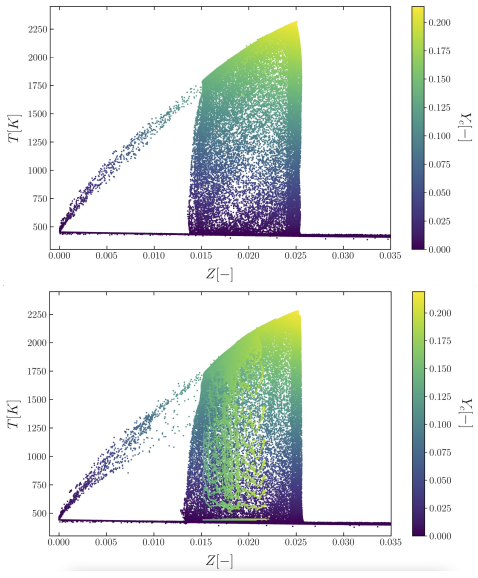

Figure 7: Conditioned temperature to the mixture fraction coloured by the progress variable. Adiabatic case (upper) and heat loss case (lower).

5. Conclusions

This study presents some preliminary results of the large-eddy simulations of a technically premixed swirl stabilized hydrogen burner with axial air injection. The burner was designed by Reichel et al. [6–9] to operate with fuel flexibility under lean conditions. The main outcomes of the experimental investigation show the axial air injection and fuel momentum contribute to FB resistance by displacing the VB further downstream. To model this behaviour, LES in the low Mach number limit with flamelet methods are used to study the main driving mechanisms leading to flame stabilization in this burner. The mixing analysis show that the central axial velocity deficit could not be overcome over the whole length of the mixing tube, leading to VB very close to the mixing tube outlet, probably promoted by a fuel-rich central zone. Regarding the influence of transport properties, different Lewis numbers did not show an effect on the iso-thermal flow. Preliminary results of the reactive flow show the flame stabilizes partially inside the mixing tube developing an increase in axial velocity along the centerline that overpredicts the experimental values. This overprediction is reduced by including heat loss and current effort is dedicated to perform further analysis and validation in this operating point considering different tabulation strategies.

Acknowledgments

The research activities conducted here have been financed by the CoEC project from the European Union's Horizon 2020 research and innovation programme under grant agreement No 952181.

References

[1] C. Tang, Y. Zhang, Z. Huang, Renewable and Sustainable Energy Reviews 30 (2014) 195–216.

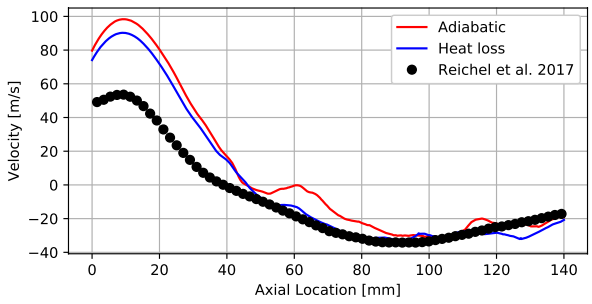

Figure 8: Comparison of the numerical simulations with the PIV data along the burner centerline.

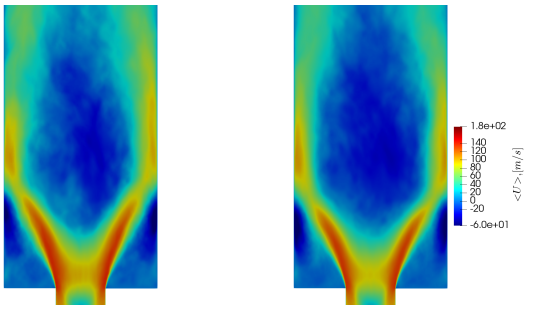

Figure 9: Mean axial velocity field for the adiabatic case (left) and heat loss (right).

[2] B. Khandelwal, A. Karakurt, P. R. Sekaran, V. Sethi, R. Singh, Progress in Aerospace Sciences 60 (2013) 45–59.
[3] K. Onarheim, I. Hannula, Y. Solantausta, Energy 199 (2020) 117337.
[4] M. C. Lee, S. B. Seo, J. H. Chung, S. M. Kim, Y. J. Joo, D. H. Ahn, Fuel 89 (2010) 1485–1491.
[5] C. Mayer, J. Sangl, T. Sattelmayer, T. Lachaux, S. Bernero, Journal of Engineering for Gas Turbines and Power 134 (2012).
[6] T. G. Reichel, S. Terhaar, C. O. Paschereit, Journal of Propulsion and Power 34 (2018) 690–701.
[7] T. G. Reichel, S. Terhaar, O. Paschereit, Journal of Engineering for Gas Turbines and Power 137 (2015).
[8] T. G. Reichel, K. Goeckeler, O. Paschereit, Journal of Engineering for Gas Turbines and Power 137 (2015).
[9] T. G. Reichel, C. O. Paschereit, International Journal of Hydrogen Energy 42 (2017) 4518–4529.
[10] S. Burmberger, T. Sattelmayer, Journal of engineering for gas turbines and power 133 (2011).
[11] T. Tanneberger, T. G. Reichel, O. Krüger, S. Terhaar, C. O. Paschereit, in: Turbo Expo: Power for Land, Sea, and Air, volume 56697, American Society of Mechanical Engineers, p. V04BT04A026.
[12] D. Mira, O. Lehmkuhl, P. Stathopoulos, T. Tanneberger, T. Reichel, C. Paschereit, M. Vázquez, G. Houzeaux, in: Turbo Expo: Power for Land, Sea, and Air, volume 51067, American Society of Mechanical Engineers, p. V04BT04A009.
[13] D. Mira, O. Lehmkuhl, A. Both, P. Stathopoulos, T. Tanneberger, T. G. Reichel, C. O. Paschereit, M. Vázquez, G. Houzeaux, Flow, Turbulence and Combustion 104 (2020) 479–507.
[14] T. Poinsot, D. Veynante, Theoretical and numerical combustion, RT Edwards, Inc., 2005.
[15] D. Mira, X. Jiang, C. Moulinec, D. Emerson, International journal of hydrogen energy 39 (2014) 7173–7189.
[16] A. Vreman, Physics of fluids 16 (2004) 3670–3681.
[17] A. Both, O. Lehmkuhl, D. Mira, M. Ortega, Computers & Fluids 200 (2020) 104436.
[18] S. Delhaye, L. Somers, J. Van Oijen, L. De Goey, Proceedings of the Combustion Institute 32 (2009) 1051–1058.
[19] Chemical-Kinetic Mechanisms for Combustion Applications, Chemical-kinetic mechanisms for combustion applications, 2016.
[20] Y. Zheng, M. Zhu, D. M. Martinez, X. Jiang, Computers & Fluids 88 (2013) 702–714.
[21] P. Domingo, L. Vervisch, D. Veynante, Combustion and Flame 152 (2008) 415–432.
[22] S. Li, Y. Zheng, L. S. Mira, D., M. Zhu, X. Jiang, J. Eng. Gas Turbines Power. 139 (2017) 031501.